2026 IEEE/SICE International Symposium on System Integration (SII)
January 11-14, 2026. Cancún, México

Dart-Throwing Teaching Device Using Force Presentation Driven by Pneumatic Artificial Muscle

Takuya Shirakawa[1,†], Tetsuro Miyazaki[1,†] and Kenji Kawashima[1]

Abstract— **In this study, we developed a fingertip motion teaching suit using pneumatic artificial muscles (PAMs) to support the acquisition of optimal release timing in dart throwing. The proposed device is equipped with bidirectional bending-type PAMs placed near the metacarpophalangeal (MP) joint of the index finger and on the back of the hand. It provides haptic guidance for finger flexion and extension through the contractile force generated by pressurization. A control algorithm is proposed to pressurize the PAM at the pre-analyzed optimal release timing while accounting for actuator delay, so that the dart is released from the fingertip grip at the intended moment. By presenting the appropriate finger extension timing synchronized with the throwing motion, the system enables intuitive training and aims to improve dart-throwing skills. To validate the effectiveness of the device, dart-throwing experiments were conducted under three conditions—before, during, and after wearing the device—with healthy adult participants. The landing error and variability in release timing were evaluated. As a result, the release timing during device use became closer to the optimal reference timing compared to the pre-wear condition, and the average landing error also decreased. In the post-wear condition, the landing error was the smallest among the three conditions for three out of four participants, and the improvement in release timing was maintained at the same level as that observed during device use. These findings suggest the presence of a retention effect and indicate that the proposed PAM-actuated device can function as an effective feedback tool for teaching motor timing.**

I. INTRODUCTION

An accurate understanding of bodily movements in sports is essential for enhancing athletic performance. This is particularly true in sports involving throwing movements, such as baseball, handball, and darts, where the ability to release an object with precise timing directly correlates with competitive success. Therefore, it is crucial to quantitatively and precisely understand and control such movements [1][2][3]. In particular, the release motion is classified as a discrete motor task, requiring high-precision timing control within a time frame on the order of a few milliseconds, making it one of the most difficult skills for beginners to master [4]. For example, in dart throwing, it is theoretically necessary to achieve a timing precision of 1.8 ms or less in order to hit a bullseye with a diameter of 4.4 cm [5], and simulation studies have suggested that to hit a target with a diameter of 20 cm from a distance of more than 6 m, the release must occur within an extremely short time window of about 1 ms [6][7]. However, the release timing is often perceived subjectively and intuitively, making it difficult for an instructor to accurately verbalize their intention and convey it to an athlete. Furthermore, it has been reported that there is a marked difference in the accuracy of perception and understanding of movement intentions between skilled performers and novices [8], which makes it difficult for instructors and learners to share a common understanding of the movement, thereby hindering efficient skill acquisition.

In addressing this issue, motion instruction has gained attention that directly appeals to bodily sensations, with methods using force feedback being particularly effective in intuitively conveying movement intentions. For example, Marchal-Crespo et al. [9] developed a device to facilitate tennis swing instruction by attaching six wires to the upper arm, which connect to an external frame, thereby guiding the arm to an ideal trajectory and demonstrating enhanced motor learning effects. In the field of rehabilitation, Sun et al. [10] have proposed systems that monitor and control lower limb movements in real-time, providing feedback on walking and running patterns to support correct motor learning, further demonstrating the efficacy of force feedback instruction in other domains. However, these systems often require large external structures or exoskeleton-like apparatuses, presenting challenges in portability, wearability, and usability.

As a solution to this issue, PAMs have attracted increasing attention in recent years. PAMs are actuators that generate contraction force through pneumatic pressure, and due to their lightweight and flexible characteristics, they have been increasingly applied to wearable haptic feedback devices [11][12]. In this study, we designed our system based on the premise that a reproducible throwing motion along a consistent average trajectory can be achieved [13][14]. The proposed system leverages the characteristics of PAMs to directly present haptic cues to the opening and closing movements of the fingers, thereby enabling motion instruction for optimal release timing in the dart-throwing task. Specifically, it consists of a single bidirectional bending-type PAM mounted on the back of the participant's hand, with the aim of guiding the fingers to open and close in accordance with the ideal release timing set by the instructor. Similar bending-type PAMs and other soft actuators have been widely used for assisting finger flexion/extension and supporting finger movements [15][16][17], and their effectiveness has been reported.

As a validation experiment, a dart-throwing task was

*This work was supported by the Bridgestone Corporation and JSPS KAKENHI Grant Number 25K14762.

† Equal contribution

[1]T. Shirakawa, T. Miyazaki and K. Kawashima are with Department of Information Physics and Computing, Graduate School of Information Science and Technology, The University of Tokyo, Japan. baichuanzuoye@gmail.com, Tetsuro_Miyazaki@ipc.i.u-tokyo.ac.jp

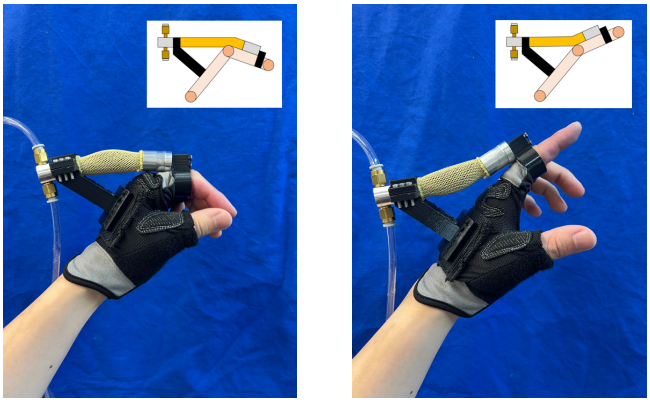

Fig. 1: Developed dart-throwing teaching suit (left: finger flexion, right: finger extension).

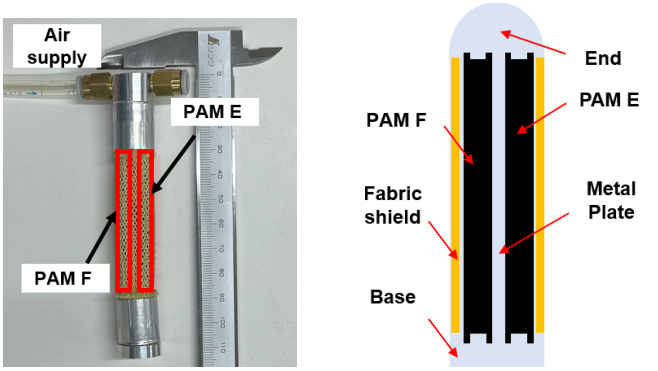

(a) The bidirectional bending-type PAM.

(b) Cross-section of bidirectional bending-type PAM.

Fig. 2: Bidirectional bending-type PAM used as the device's actuator.

conducted with four healthy adult participants under three conditions: without PAM, with PAM, and after PAM removal. The variability and reproducibility of the release timing were compared among the three conditions for each participant.

II. MATERIALS AND METHOD

A. Design of Assistive Suit

In this study, we developed a suit-type device that enables motion instruction for optimal release timing in dart-throwing. An overview of the developed dart-throwing teaching suit is shown in Fig. 1. The prototype suit comprises a ring component attached around the MP joint of the index finger, a base component fixed to the back of the hand, and the bidirectional bending-type PAM.

We adopted a bidirectional bending-type PAM instead of linear PAMs because a single bending-type actuator can generate both flexion and extension, whereas a linear configuration would require two PAMs to realize bidirectional motion. Such a dual-actuator arrangement would increase the mass and bulk around the hand, potentially hindering natural finger motion and reducing the overall wearability of the device. Based on these considerations, the bending-type PAM was deemed more suitable for the present application.

It is designed to induce the opening and closing of the finger grasping the dart in accordance with the optimal release timing, which is pre-analyzed based on the trainee's average throwing trajectory. Fig. 2 shows the bending-type PAM used in the device, which was provided as a prototype by Bridgestone Corporation. The bidirectional PAM has two PAMs: PAM F, which induces finger flexion, and PAM E, which induces finger extension. These inner pressures are P_{F} and P_{E}, and are controlled to generate the torque for the index finger opening and closing. The two ends of the PAM are fixed to the ring and base components, respectively, allowing the device to be worn by the trainee. All fixing components were fabricated with PLA material using a fused deposition modeling (FDM) type 3D printer. This structure enables the application of assistive forces for both flexion and extension directions of the index finger by pressurizing and depressurizing the PAM.

To inform the design of the device, we first conducted a preliminary experiment to measure the angular variation range of the MP joint during dart-throwing by skilled athletes. The result of the preliminary experiment is presented in Fig. 3. The acquired time-series data of MP joint angles were processed using a two-stage filtering; a five-point median filter was first applied to suppress spike noise, followed by a five-point moving average filter for temporal smoothing. The resulting joint angle is denoted as θ_{MP} [deg], and its range of motion was 115 to 155 deg.

In the geometric modeling of the device, we define θ_{p} as the angle between the PAM and the supporting structure oriented dorsally, as illustrated in Fig. 4. Due to the filling characteristics of the PAM, which affect bending behavior, the device was designed to allow a maximum bending of 20 deg in either flexion or extension, supplemented by mechanical support structures to cover the remaining range of motion. To achieve approximately 45 deg of extension from the closed-finger state ($\theta_{\mathrm{MP}} = 115$ deg), the base component must provide sufficient width and height with respect to the MP joint. To satisfy this requirement, we defined the geometric configuration of the base and PAM connection point based on the schematic in Fig. 4. The angle θ_{p} is treated as a design reference. Considering the anthropometric data of the user, the distance from the finger-side attachment to the MP joint was set to $L_2 = 22.0$ mm, and the effective PAM length (hypotenuse) was set to $L_1 + l_2 = 76.0$ mm. Based on the Pythagorean theorem, the attachment point on the back of the hand was determined as follows:

$$l_{\mathrm{h}} = (L_1 + l_2)\sin\theta_{\mathrm{p}} \ , \tag{1}$$

$$l_{\mathrm{w}} = (L_1 + l_2)\cos\theta_{\mathrm{p}} \ . \tag{2}$$

In this study, the design angle was set to $\theta_{\mathrm{p}} = 45$ deg, resulting in both l_{h} and l_{w} being 53.7 mm. The base component was designed accordingly.

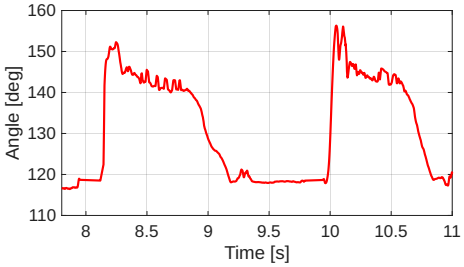

Fig. 3: Range of motion of the MP joint of the index finger in a representative participant.

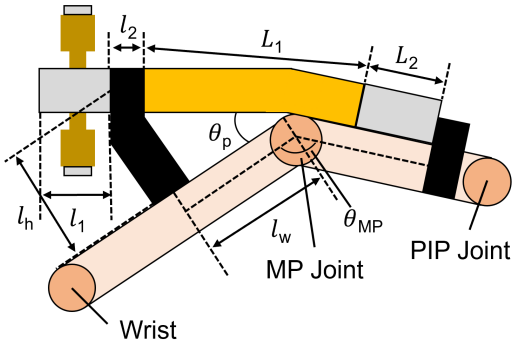

Fig. 4: Schematic diagram of the fabricated device, illustrating the geometric configuration for generating bending assistance around the MP joint of the index finger.

B. System Overview

Fig. 5 illustrates the schematic of the index finger flexion–extension instruction system developed in this study. This system operates under the assumption that the time-series data of the participant's elbow joint angle, $\theta_e(t)$, has been pre-acquired. t [s] is time. While receiving haptic feedback from the assistive device via the contraction force generated by the attached PAM, the participant throws a dart, thereby learning the optimal release timing. The positions of the elbow, shoulder, and dart are measured in real time using a motion capture system (Miqus M3, Qualisys) with a sampling frequency of 500 Hz. The acquired marker coordinates are transmitted via the Virtual Reality Peripheral Network (VRPN) to a PAM control PC. On the control PC, the timing at which the elbow joint angle $\theta_e(t)$ reaches a local minimum below 30 deg is defined as $t = 0$. The finger extension is then initiated at the optimal release time t_{opt}, which is calculated from the mean motion trajectory. Specifically, the system compensates for the PAM response delay τ_{PAM} and switches the servo valve at $t = t_{opt} - \tau_{PAM}$ to regulate the internal pressure. All control algorithm is implemented using the Robot Operating System (ROS).

C. Calculation of applied pressure to the PAM

Achieving a bending angle of approximately ± 20 deg with the bidirectional bending PAM is sufficient to meet the range-of-motion requirements (total 40 deg) shown in Section II-A. Therefore, we aim to determine the driving pressure required for the PAM to achieve a one-sided bending of 20 deg, and

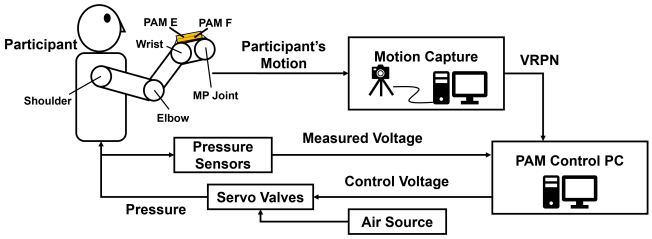

Fig. 5: System overview of the index-finger flexion/extension motion teaching setup using force feedback.

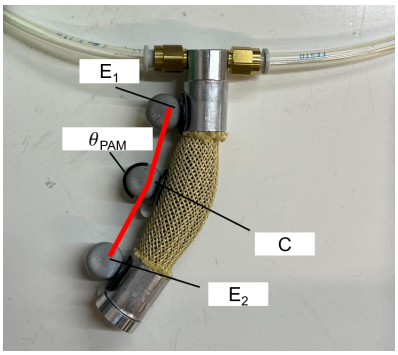

Fig. 6: Measurement setup for evaluating the bending angle θ_{PAM} of the bidirectional bending-type PAM.

we conducted an experiment to measure the bending angle θ_{PAM}. The experimental setup is shown in Fig. 6. To calculate the bending angle, we used the measured marker positions placed at the center and both ends of the PAM. The position vectors of the markers at time t are defined as $\mathbf{p}_C(t)$, and $\mathbf{p}_{E_1}(t)$, $\mathbf{p}_{E_2}(t)$. As shown in Fig. 6, the vectors from the center marker C to each of the end markers E_1 and E_2 are defined as follows:

$$\mathbf{v}_1(t) = \mathbf{p}_{E_1}(t) - \mathbf{p}_C(t) \ , \tag{3}$$

$$\mathbf{v}_2(t) = \mathbf{p}_{E_2}(t) - \mathbf{p}_C(t) \ . \tag{4}$$

The PAM bending angle $\theta_{PAM}(t)$ is then calculated as the angle between vectors $\mathbf{v}_1(t)$ and $\mathbf{v}_2(t)$ using the cosine law based on the inner product:

$$\theta_{PAM}(t) = \cos^{-1}\left(\frac{\mathbf{v}_1(t)^\top \mathbf{v}_2(t)}{\|\mathbf{v}_1(t)\| \, \|\mathbf{v}_2(t)\|} \right) \ . \tag{5}$$

In the experiment, we applied Eq. (5) to the data of $\theta_{PAM}(t)$ sampled at 500 Hz, corresponding each bending angle to the applied pressure history. As shown in Fig. 7, applying a driving pressure of $P_E = 360$ kPa (with $P_F = 0$ kPa) resulted in θ_{PAM} moved from 175 to 155 deg, and the target motion range of 20 deg was achieved. Therefore, we adopted 360 kPa as the driving pressure in the subsequent experiments. Fig. 7 also shows the input voltage of the servo valve that shows the start timing of pressurization. We set the voltage threshold to detect the pressure input timing and the angular velocity threshold of 1.0 deg/s to detect the start of bending motion. Using the above thresholds, we confirmed that the response delay of the device was 48 ms which is the time lag between red and blue dashed lines in Fig. 7.

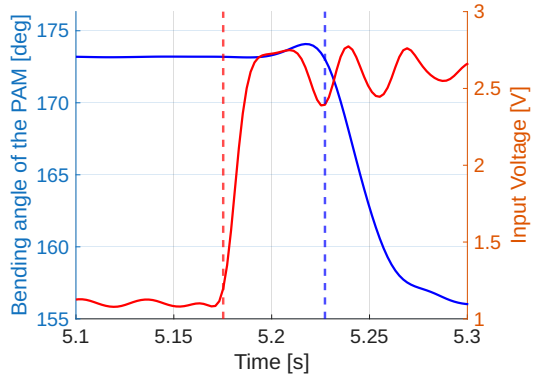

Fig. 7: Angle response of a standalone bidirectional bending-type PAM.

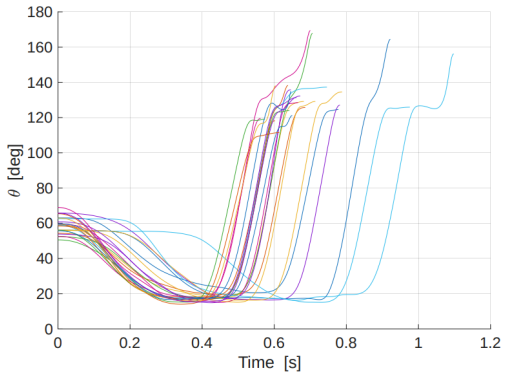

Fig. 8: Arranged elbow-angle plot.

D. Calcuation of reference profile

To quantitatively analyze the upper limb motion during dart-throwing, optical markers were attached to the participant's shoulder and elbow joints, and an additional marker was affixed to the rear end of the dart. The participant performed 25 dart throws while holding the dart, and three-dimensional motion data were acquired using a motion capture system. At each time point t in each trial, the motion vectors of the upper arm and forearm, referenced from the elbow joint, were defined as follows:

$$\mathbf{v}_{\mathrm{u}}(t) = \mathbf{p}_{\mathrm{s}}(t) - \mathbf{p}_{\mathrm{e}}(t) \ , \tag{6}$$

$$\mathbf{v}_{\mathrm{d}}(t) = \mathbf{p}_{\mathrm{w}}(t) - \mathbf{p}_{\mathrm{e}}(t) \ , \tag{7}$$

where $\mathbf{p}_{\mathrm{s}}(t)$, $\mathbf{p}_{\mathrm{e}}(t)$, and $\mathbf{p}_{\mathrm{w}}(t)$ represent the three-dimensional position vectors of the shoulder, elbow, and wrist, respectively. The elbow joint angle $\theta_{\mathrm{e}}(t)$ was calculated based on Eq. (5).

The raw data obtained from the 25 trials contained variations in throwing timing and outlier trajectories. To enable consistent comparison of the angular changes from motion onset to completion, a waveform normalization procedure was applied. First, the time at which the elbow joint angle reached its minimum value was defined as t_{min}. In the segment $t < t_{\mathrm{min}}$, the time at which the angle reached its local maximum was redefined as the new time origin $t = 0$, representing the motion onset. Similarly, in the segment $t > t_{\mathrm{min}}$, the time at which the angle reached the subsequent local maximum was defined as the motion endpoint, and the interval between these two points was extracted as the effective trajectory. To enhance the accuracy of robust peak detection, a moving average filter with a window size of $N = 11$ was applied to the extracted angular waveforms, thereby reducing high-frequency noise. As a result, we obtained 25 arranged elbow-angle trajectories as shown in Fig. 8.

For each processed trial i, the mean trajectory $\bar{\theta}_{\neg i}(t)$ of the remaining 24 trials was computed, and the reproducibility of the waveforms was quantitatively evaluated using the root mean square error (RMSE) defined as:

$$\mathrm{RMSE}_i = \sqrt{\frac{1}{T}\sum_{t=1}^{T}\left(\theta_i(t) - \bar{\theta}_{\neg i}(t)\right)^2} \ , \tag{8}$$

where T denotes the number of samples in each trajectory. Trials with $\mathrm{RMSE}_i > \mathrm{RMSE}_{\mathrm{th}}$ were classified as outliers, where the empirical threshold was set to $\mathrm{RMSE}_{\mathrm{th}} = 20$ deg, and were excluded from further analysis.

For the remaining N reproducible elbow joint angle trajectories $\theta_i(t)$ $(i = 1, \ldots, N)$, time normalization was performed by dividing each trajectory by its length T_i:

$$u = \frac{t}{T_i}, \quad 0 \le u \le 1 \ . \tag{9}$$

Each normalized trajectory was interpolated using the Piecewise Cubic Hermite Interpolating Polynomial (PCHIP) method to obtain an equally spaced vector $\hat{\theta}_i(u_j)$ with $N_{\mathrm{norm}} = 200$ points $(j = 1, \ldots, 200)$. These were arranged into a matrix $M \in \mathbb{R}^{N\times 200}$, from which the column-wise mean and standard deviation were calculated as:

$$\bar{\theta}_{\mathrm{e}}(u_j) = \frac{1}{N}\sum_{i=1}^{N} M_{i,j} \ , \tag{10}$$

$$\sigma_\theta(u_j) = \sqrt{\frac{1}{N-1}\sum_{i=1}^{N}\left(M_{i,j} - \bar{\theta}_{\mathrm{e}}(u_j)\right)^2} \ . \tag{11}$$

Using the mean segment length

$$\bar{T} = \frac{1}{N}\sum_{i=1}^{N} T_i \ , \tag{12}$$

the normalized time u_j was converted to the real time axis by $t_j = u_j\bar{T}$, yielding the representative elbow angle waveform $\bar{\theta}_{\mathrm{e}}(t_j)$.

The same processing steps were applied to the 3D position data of the dart's rear-end marker. The x–z plane trajectory of each trial was expressed as $\mathbf{p}_i(u) = \left[x_i(u), z_i(u)\right]^\top$ and normalized and interpolated to derive the representative trajectory:

$$\bar{\mathbf{p}}(u) = \frac{1}{N}\sum_{i=1}^{N}\mathbf{p}_i(u) \ . \tag{13}$$

The resulting $\bar{\theta}_e(t)$ and $\bar{\mathbf{p}}(u)$ were used as reference profiles for calculating the optimal release timing and for designing the control law of the suit.

E. Estimation of the optimal release timing

Based on the representative average dart trajectory derived in the previous section, this section calculates the predicted landing position of the dart for each possible release time and defines the optimal release timing t^* as the time point that minimizes the vertical error from the target position. First, the dart tip position $(x(t),\, z(t))$ at each time t is extracted, and the velocity vector $(v_{x0}(t),\, v_{z0}(t))$ is approximated using the following finite differences:

$$v_{x0}(t) \approx (x(t+\delta) - x(t))/\delta \ , \tag{14}$$

$$v_{z0}(t) \approx (z(t+\delta) - z(t))/\delta \ , \tag{15}$$

where δ is the time interval 0.002 s. Assuming a simple projectile motion in the vertical plane that neglects air resistance and rotation, the subsequent flight is modeled as:

$$x_{\text{hit}}(t) = x_0(t) + v_{x0}(t) \cdot \Delta t \ , \tag{16}$$

$$z_{\text{hit}}(t) = z_0(t) + v_{z0}(t) \cdot \Delta t - \frac{1}{2} g \cdot (\Delta t)^2 \ , \tag{17}$$

where $(x_0(t), z_0(t))$ denotes the release position, and Δt is the flight time, estimated from the horizontal distance to the target and the initial velocity as:

$$\Delta t = (x_{\text{target}} - x_0(t))/v_{x0}(t) \ . \tag{18}$$

Given the target position $(x_{\text{target}}, z_{\text{target}})$, the vertical error $e(t)$ at release time t is defined as:

$$e(t) = |z_{\text{hit}}(t) - z_{\text{target}}| \ . \tag{19}$$

By calculating this error $e(t)$ for all candidate time points t, the time that minimizes this error is defined as the optimal release timing t^*:

$$t^* = \arg\min_t e(t) \ . \tag{20}$$

The derived t^* maximizes vertical hitting accuracy relative to the target and is used as the trigger timing for haptic feedback in the proposed instruction system.

F. Pressure controller

An open-loop control strategy was adopted, wherein pressure is switched based on a predetermined timing for actuating the device. In the initial state, when the participant is holding the dart, the pressures are set to maintain a flexed posture of the finger as follows:

$$P_{\text{F}}(t) = 360 \text{ kPa}, \ P_{\text{E}}(t) = 0 \text{ kPa}. \tag{21}$$

The release timing is determined based on the optimal release time t^*, defined in the previous section as the timing that minimizes the dart's landing error in a projectile motion model. In practice, PAM actuation is subject to multiple delays, including valve response, pressure transmission, and mechanical deformation. In this study, the overall response delay of the device was experimentally measured to be $\tau_{\text{PAM}} = 48$ ms, as shown in Fig. 7. Accordingly, the pressure switching trigger time is compensated as

$$t_{\text{trigger}} = t^* - \tau_{\text{PAM}} \ . \tag{22}$$

At t_{trigger}, the pressures are switched as:

$$P_{\text{F}}(t) = \begin{cases} 360 \text{ kPa}, & t < t_{\text{trigger}} \\ 0 \text{ kPa}, & t \geq t_{\text{trigger}} \end{cases} \ , \tag{23}$$

$$P_{\text{E}}(t) = \begin{cases} 0 \text{ kPa}, & t < t_{\text{trigger}} \\ 360 \text{ kPa}, & t \geq t_{\text{trigger}} \end{cases} \ . \tag{24}$$

This switching induces finger extension, facilitating dart release.

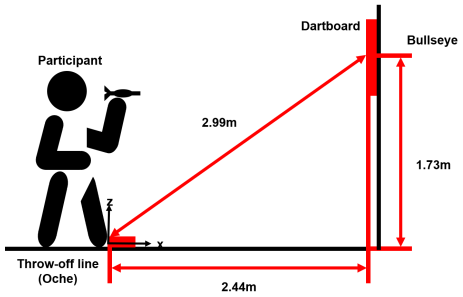

Fig. 9: The position of the participant aiming the dartboard.

III. EXPERIMENT

To evaluate the effectiveness of the proposed suit, experiments were conducted with four healthy adult male participants. The study was approved by the Ethics Committee of the Graduate School of Information Science and Technology, The University of Tokyo (Approval No. UT-IST-RE250402-2), and informed consent was obtained from the participants.

The participant performed a dart-throwing task under conditions consistent with standard soft dart rules. As illustrated in Fig. 9, the dartboard was placed such that the bullseye was located 1.73 m above the floor, and the horizontal distance from the throw-off line to the board surface was set to 2.44 m. The participants were allowed to adopt a self-selected throwing posture and was instructed to consistently aim at the center of the bullseye (diameter: 44 mm).

As preliminary trials, each participant performed 25 dart throws. Outlier removal was performed, and trials with RMSE exceeding $\text{RMSE}_{\text{th}} = 20$ deg were excluded. The remaining valid trials were averaged to obtain a representative trajectory $\bar{\theta}_e(t)$ corresponding to a typical throwing motion. For controlling the suit, the optimal release timing t^* was employed. An open-loop control scheme was implemented as described in the previous section.

In the main experiment, each participant performed two sets of ten dart throws under each of three conditions: before wearing the instructional suit (BW), while wearing it (WW), and after wearing it (AW). A total of 60 dart throws were recorded. For each trial, both the dart landing position and throwing kinematics were analyzed to assess the instructional effect of the proposed system.

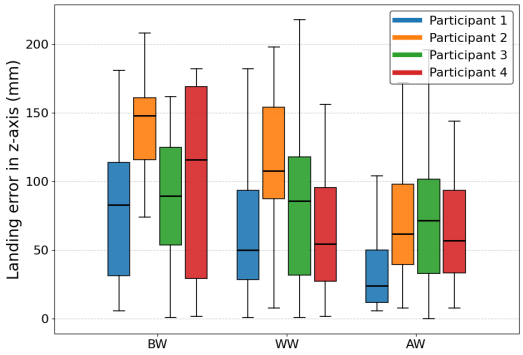

Fig. 10: Box plot of deviations along the Z directions, with outliers excluded based on the 1.5×IQR criterion.

TABLE I: Optimal Release Timing for Each Participant.

Participant	Optimal release timing t^* (ms)
1	126.0
2	235.0
3	138.0
4	214.0

IV. RESULTS

The mesian and variance of the absolute values of the z-coordinates were calculated under three conditions, and these values are shown in Fig. 10. Outliers were excluded from the box plots, where outliers are defined as values that lie beyond 1.5 times the interquartile range (IQR) from the upper or lower quartile. The mesian z-coordinates decreased during and after device usage. The variance increased during the WW condition compared to the other two conditions, which may be attributed to interference between the device and natural human motion during the motion learning process. Finally, the AW condition's variance became small. These results suggest the effectiveness of the proposed training.

Furthermore, the release timing was defined as the moment when the rate of change in the distance between the elbow and the dart exceeded zero, and the optimal release timing for each participant was shown in Table I. The mean and unbiased variance of the release timing were calculated for each phase, as shown in Table II. The condition of BW indicates high variability. In contrast, the WW condition confirms that the system enabled more accurate and consistent releases. Additionally, the AW condition indicates that the motion pattern acquired during device use was retained. These results suggest that the proposed suit is not only a temporary assistive tool but may also serve as an effective device for supporting motor learning.

V. CONCLUSIONS

We proposed a PAM-actuated haptic feedback system designed to provide motion instruction for dart throwing and evaluated its effectiveness. The experimental results demonstrated improvements in the average landing position, and the release timing approached the optimal value computed from the representative mean trajectory. These findings suggest that the proposed system is effective in reducing vertical landing error. Future work will include validating the method with a more diverse population of participants and extending the system to full three-dimensional motion to further assess its generalizability and practical applicability.

TABLE II: Statistics of Release Timing.

		Before Wearing	**While Wearing**	**After Wearing**
Participant 1	Mean (ms)	329.8	116.0	216.9
	Variance (ms^2)	2.12×10^5	1.71×10^3	3.08×10^3
Participant 2	Mean (ms)	465.1	176.9	184.0
	Variance (ms^2)	2.37×10^5	2.30×10^4	1.39×10^4
Participant 3	Mean (ms)	158.5	160.4	139.9
	Variance (ms^2)	7.73×10^4	8.01×10^3	1.22×10^3
Participant 4	Mean (ms)	69.1	93.2	103.9
	Variance (ms^2)	1.25×10^3	3.14×10^3	1.76×10^3

ACKNOWLEDGMENT

We are grateful for Shingo Oono's technical assistance with the Bridgestone Corporation.

References

[1] Stodden, D. F., Fleisig, G. S., McLean, S. P., Andrews, J. R.: "Relationship of biomechanical factors to baseball pitching velocity: within pitcher variation," *Journal of Applied Biomechanics*, vol. 21, no. 1, pp. 44–56, 2005.

[2] Nasu, D., Matsuo, T., Kadota, K.: "Two types of motor strategy for accurate dart throwing," *PLoS ONE*, vol. 9, no. 2, e88536, 2014.

[3] van den Tillaar, R., Cabri, J.: "Kinematics of overarm throwing in handball and the influence of instructional constraints," *Journal of Sports Sciences*, vol. 30, no. 8, pp. 801–815, 2012.

[4] Schmidt, R. A., Lee, T. D.: *Motor Control and Learning: A Behavioral Emphasis*, 6th ed., Human Kinetics, 2019.

[5] Smeets, J. B. J., Frens, M. A., Brenner, E.: "Throwing darts: timing is not the limiting factor," *Experimental Brain Research*, vol. 144, no. 2, pp. 268–274, 2002.

[6] Calvin, W. H.: "A stone's throw and its launch window: timing precision and its implications for language and hominid brains," *Journal of Theoretical Biology*, vol. 104, no. 1, pp. 121–135, 1983.

[7] Chowdhary, A. G., Challis, J. H.: "Timing accuracy in human throwing," *Journal of Theoretical Biology*, vol. 201, no. 4, pp. 219–229, 1999.

[8] Abernethy, B.: "Expert–novice differences in perception: How expert does expert need to be?" *Research Quarterly for Exercise and Sport*, vol. 61, no. 3, pp. 238–245, 1990.

[9] Marchal-Crespo, L., van Raai, M., Rauter, G., et al.: "The effect of haptic guidance and visual feedback on learning a complex tennis task," *Experimental Brain Research*, vol. 231, pp. 277–291, 2013.

[10] Sun, W., Lin, J. W., Su, S. F., et al.: "Reduced adaptive fuzzy decoupling control for lower limb exoskeleton," *IEEE Transactions on Cybernetics*, vol. 51, no. 3, pp. 1099–1109, Mar. 2021.

[11] Miyazaki, T., Kawase, T., Kanno, T., et al.: "Running motion assistance using a soft gait-assistive suit and its experimental validation," *IEEE Access*, vol. 9, pp. 94700–94713, 2021.

[12] Hayashi, H., Kawase, T., Miyazaki, T., et al.: "Online assistance control of a pneumatic gait assistive suit using physical reservoir computing exploiting air dynamics," *Proc. IEEE International Conference on Robotics and Automation (ICRA)*, pp. 3245–3251, Philadelphia, PA, USA, 2022.

[13] Kasuga, S., et al.: "High intra-task and low inter-task correlations of motor performance across repeated motor tasks," *Scientific Reports*, vol. 12, pp. 12345, 2022.

[14] Srinivasan, D.: "Motor variability in occupational health and performance," *Clinical Biomechanics*, vol. 27, no. 10, pp. 979–993, 2012.

[15] Al-Fahaam, H., Davis, S., Nefti-Meziani, S.: "The design and mathematical modelling of novel extensor bending pneumatic artificial muscles (EBPAMs) for soft exoskeletons," *Frontiers in Robotics and AI*, vol. 4, pp. 1–14, 2018.

[16] McCall, R., Al-Fahaam, H., Davis, S., Nefti-Meziani, S.: "Soft pneumatic actuators for pushing fingers into extension," *Actuators*, vol. 13, no. 1, pp. 1–15, 2024.

[17] Wirekoh, J., et al.: "Design of fiber-reinforced soft bending pneumatic artificial muscles," *Soft Robotics*, vol. 8, no. 5, pp. 524–537, 2021.